COMMUNICATION

CrossMark
← click for updates

Dislocation strain as the mechanism of phonon scattering at grain boundaries

Hyun-Sik Kim,[abc] Stephen D. Kang,[ab] Yinglu Tang,[abd] Riley Hanus[a] and G. Jeffrey Snyder*[ab]

Thermal conductivities of polycrystalline thermoelectric materials are satisfactorily calculated by replacing the commonly used Casimir model (freqency-independent) with grain boundary dislocation strain model (frequency-dependent) of Klemens. It is demonstrated that the grain boundaries are better described as a collection of dislocations rather than perfectly scattering interfaces.

Reduction of lattice thermal conductivity has been one of the most productive routes towards improving thermoelectric figure of merit,[1] $zT = S^2\sigma T/\kappa$ where S, σ, T, and κ are the Seebeck coefficient, electrical conductivity, temperature and the thermal conductivity, respectively. The thermal conductivity, κ, can be attributed to heat transported along with the conduction of electrons and holes (κ_e), and from phonons (lattice vibrations) travelling through the lattice (κ_l). The lattice thermal conductivity, κ_l, can be suppressed with disorder among many length scales, ranging in size from as small as an atom (point-defect scattering) up to a few millimetres (boundary scattering).[2] Especially, the effects of boundary scattering are of utmost importance for thermoelectric performance.

Boundary scattering was first observed in a single crystal by de Haas and Biermasz.[3] The phonon scattering at sample boundaries was explained by Casimir[4] who suggested that the phonon mean free path (MFP) could be approximated as the sample size (frequency-independent). The frequency independence of the Casimir model means that the sample boundaries are just as effective at limiting the MFP of short wavelength phonons as they are for long wavelength phonons. The Casimir model could be considered phenomenological, in the sense that it does not specify a real condition (at the atomic level) of the interface.

[a] *Department of Materials Science and Engineering, Northwestern University, Evanston, Illinois 60208, USA. E-mail: jeff.snyder@northwestern.edu*

[b] *Department of Applied Physics and Materials Science, California Institute of Technology, Pasadena, California 91125, USA*

[c] *Materials Research Center, Samsung Advanced Institute of Technology, Samsung Electronics, Suwon 443-803, South Korea*

[d] *The Swiss Federal Laboratories for Materials Science and Technology, Überlandstrasse 129, 8600 Dübendorf, Switzerland*

Conceptual insights

For 50 years, we have commonly been using Casimir's theory that describes the scattering of heat-carrying lattice vibrations (phonons) on the sample boundaries to also describe the reduction of thermal conductivity due to grain boundaries. In the frequency-independent Casimir model, phonons simply cannot travel across the boundaries, which is not the case in grain boundaries. This and a growing body of experimental and computational evidence shows that phonon scattering at grain boundaries is more complex than previously assumed. However, the precise mechanism of phonon scattering at grain boundaries is unknown. Here we show that frequency-dependent grain boundary dislocation strain scattering may be responsible. The conceptual insight here is that the grain boundary dislocation strain model can substitute for the Casimir model. More importantly, the two models can be distinguished at low temperature in fine-grained materials such that experimental evidence supports the grain boundary dislocation strain model. In this way, we suggest that grain boundaries themselves are best conceptualized as a collection of dislocations, which opens novel possibilities for materials design.

Berman suggested that scattering of phonons at grain boundaries could limit the MFP the same way phonon scattering on sample boundaries did, and since then the grain size of polycrystalline materials has been adopted as the MFP in the Casimir model (also known as grey model).[5,6] Although it may be suitable to use sample dimension as the MFP due to perfect acoustic mismatch at perfectly rough sample surfaces, it is not entirely appropriate for grain size because adjacent grains have similar acoustic impedance.

Recently, Wang *et al.* demonstrated that the grey model failed to explain the κ_l of nanocrystalline silicon.[7] At low temperature, it was observed that the measured κ_l followed a T^2 trend instead of a T^3, which was predicted in the grey model. This result implies a MFP that depends on frequency as $\Lambda_B{}^{-1} \sim \omega$, where Λ_B and ω are the boundary scattering MFP and phonon frequency, respectively.

Frequency-dependent Λ_B was first introduced by Ziman in an attempt to apply the Casimir model to materials with real boundaries.[8] Roughness of sample boundaries was taken into consideration in a frequency-dependent specularity term included

in the Λ_B. However, the Ziman model did not predict $\Lambda_B^{-1} \sim \omega$; it can be considered a phenomenological term. Hua and Minnich[9] successfully predicted Wang et al.'s results via Monte Carlo simulations which included frequency-dependent phonon transmissivity at grain boundaries[7] (consistent with $\Lambda_B^{-1} \sim \omega$). The frequency-dependent interfacial (Kapitza) resistance of grain boundaries manifested itself even in molecular-dynamics simulations.[10,11] For example, Young and Maris[12] found phonon transmission coefficient decreasing with increasing frequency for the Kapitza resistance at an interface between two dissimilar solids. Moreover, the thermal conduction in thin films was commonly depicted with Fuchs–Sondheimer equation with the frequency-dependent specularity term from the Ziman model.[13–15] Unfortunately, above models and simulations for frequency-dependent Λ_B are only phenomenological without any mechanisms because they do not specify real conditions of the boundaries.

In this work, we propose that interface scattering could be due to strain at grain boundaries described analytically as dislocation strain as formulated by Klemens.[16] Here we show that the κ_l calculated previously with the grey model can be equally satisfactorily modelled with Klemens' grain boundary dislocation scattering term by using appropriate value for dislocation density. A most promising example is a recent demonstration of exceptional zT ($\sim$1.86 at 320 K) in $Bi_{0.5}Sb_{1.5}Te_3$ where grain boundary dislocations are produced by liquid-phase compaction.[17] The grey model plus dislocation scattering we used in Kim et al.[17] is here entirely replaced by the dislocation scattering. The dislocation model demonstrates its superiority by predicting a T^2 trend instead of the T^3 of the grey model for the nanocrystalline silicon[7] system of Wang et al.

Finally we show that the Klemens model suggests dislocation boundary scattering can be enhanced by engineering compositional changes around dislocations in alloys as observed in silicon–germanium alloys[18–20] (not predicted by Casimir model).

Models for phonon scattering

From the kinetic theory of gases, the lattice thermal conductivity (κ_l) can be expressed as arising from the heat capacity of phonons (C), phonon velocity (v), and total relaxation time (τ_{total}), as a function of ω such that

$$\kappa_l = \frac{1}{3}\int C(\omega)v^2(\omega)\tau_{total}(\omega)d\omega. \quad (1)$$

Using the Debye model (phonon group velocity is constant), Callaway's equation for the κ_l becomes

$$\kappa_l = \frac{k_B}{2\pi^2 v}\left(\frac{k_B T}{\hbar}\right)^3 \int_0^{\theta/T} \frac{\tau_{total}(z)z^4 e^z}{(e^z-1)^2}dz, \quad (2)$$

where k_B, $\hbar$, θ, and z are the Boltzmann constant, reduced Planck's constant, Debye temperature, and $\hbar\omega/k_B T$, respectively.[21] The κ_l of a material can be calculated using eqn (2), once its $\tau_{total}(z)$ is determined from individual relaxation times (τ_i) for different scattering processes according to Matthiessen's rule

$$\tau_{total}(z)^{-1} = \sum_i \tau_i(z)^{-1} = \tau_U^{-1} + \tau_{PD}^{-1} + \tau_B^{-1}. \quad (3)$$

Relaxation times associated with Umklapp scattering (τ_U), point-defect scattering (τ_{PD}), and frequency-independent boundary scattering (τ_B), which assumes completely inelastic (specularity zero) scattering at the grain boundaries are most commonly considered. The τ_B has been found to be a good model for surfaces (of nanowires for instance) where there is perfect acoustic mismatch at the interface between the material and vacuum. Frequency-independent τ_B is given by[22]

$$\tau_B^{-1} = \frac{v}{d}, \quad (4)$$

where d is the experimentally determined grain size. Umklapp scattering occurs when phonons in a crystal are scattered by other phonons. Its relaxation time is of the form[22]

$$\tau_U^{-1} = A_N \frac{2}{(6\pi^2)^{1/3}}\frac{k_B V^{1/3}\gamma^2\omega^2 T}{Mv^3}, \quad (5)$$

where V, γ, and M are the atomic volume, Grüneisen parameter, and the atomic mass. The parameter A_N takes normal phonon–phonon scattering (total crystal momentum conserving process) into account.[23] Point-defect scattering arises from an atomic size disorder in alloys. The disorder is described in terms of the scattering parameter (Γ) within the τ_{PD} formula as[24]

$$\tau_{PD}^{-1} = \frac{V\omega^4}{4\pi v^3}\Gamma. \quad (6)$$

In eqn (6), Γ is related to the difference in mass (ΔM) and lattice constant (Δa) between two constituents of an alloy as[25]

$$\Gamma = x(1-x)\left[\left(\frac{\Delta M}{M}\right)^2 + \frac{2}{9}\left\{(G+6.4\gamma)\frac{1+r}{1-r}\right\}^2\left(\frac{\Delta a}{a}\right)^2\right], \quad (7)$$

where x and r are the fractional concentration of either of constituents and the Poisson ratio, respectively. The parameter G represents material dependent $(\Delta K/K)(R/\Delta R)$ where ΔK and ΔR are the contrast in the bulk modulus and that in the local bond length, respectively. The G was regarded as an adjustable parameter in the calculation.

Phonon scattering of dislocations in a grain boundary can be treated as resulting from scattering by dislocation cores (τ_{DC}) and by the dislocation strain (τ_{DS}) as[16,26]

$$\tau_{DC}^{-1} = \left(\frac{2}{sd}\right)\frac{V^{4/3}}{v^2}\omega^3, \quad (8)$$

$$\tau_{DS}^{-1} = 0.6 \times B_{D,eff}^2\left(\frac{2}{sd}\right)(\gamma+\gamma_1)^2\omega\left[\frac{1}{2} + \frac{1}{24}\left(\frac{1-2r}{1-r}\right)^2\right.$$
$$\left.\times\left\{1 + \sqrt{2}\left(\frac{v_L}{v_T}\right)^2\right\}^2\right], \quad (9)$$

where $B_{D,eff}$, γ, γ_1, v_L, and v_T are the magnitude of effective Burgers vector, Grüneisen parameter, change in Grüneisen parameter, longitudinal phonon velocity, and the transverse phonon velocity, respectively. The change in Grüneisen parameter (γ_1) in τ_{DS}^{-1} describes the modulation of solute atom concentration by strain fields around dislocations in alloys.

Initially, Klemens derived eqn (8) and (9) for collections of single dislocations (with density N_D) within a grain. As dislocations could be easily introduced into grains by deformation, Klemens' equations were often used to compute κ_l of strained materials.[27,28] When arrays of dislocations at boundaries (or interfaces) were found physically equivalent to a sum of individual dislocations within a grain,[8] κ_l reductions from dislocations, which originated due to lattice mismatch between thin film and substrate,[29] or between different phases in poly-crystalline materials[30] were explained by Klemens' equations. Nevertheless, the consideration of the scattering effect of dislocation arrays at grain boundaries of single-phase polycrystalline materials has been scarce. Here we replace the density of dislocations per unit area (N_D) used by Klemens with $N_D \approx 2/(d \times s)$, where d is the average grain size and s is the average spacing between dislocation cores in order to apply Klemens equations to phonon scattering of grain boundary dislocations where average grain size can be an observed parameter.

Dislocation scattering can explain thermal conductivity without the need for boundary scattering

Recently, a dramatic zT improvement in $Bi_{0.5}Sb_{1.5}Te_3$ was attributed to substantially low κ_l.[17] In ref. 17 we showed that modelling the boundary scattering with the normally expected τ_B^{-1} along with the experimentally determined $\tau_U^{-1} + \tau_{PD}^{-1}$ was insufficient to explain the low κ_l of $Bi_{0.5}Sb_{1.5}Te_3$ with dense dislocation arrays at grain boundaries. The additional scattering mechanisms, τ_{DC}^{-1} and τ_{DS}^{-1} from dislocations were required to explain the κ_l. In this section we show that within the range of physically reasonable parameters, once dislocation scattering is included, since an array of dislocations situated in the plane makes a grain boundary[31] the traditional boundary scattering τ_B^{-1} is not necessary to satisfactorily model the data.

In ref. 17 various forms of $Bi_{0.5}Sb_{1.5}Te_3$ samples were considered to self-consistently model the κ_l. The parameters A_N and G in τ_U^{-1} and τ_{PD}^{-1} (eqn (5) and (6)), respectively were determined by fitting the modelled κ_l to the experimental κ_l of large grained $(Bi_{1-x}Sb_x)_2Te_3$ alloys[32] with varying x. The use of reliable literature values determined experimentally, eliminates or minimizes the parameters needed for the κ_l calculation.

The κ_l of the samples fabricated via different processing routes (Ball milling: BM, melt spun with stoichiometric tellurium: S-MS, and melt spun with excess tellurium: Te-MS) were modelled

using the τ_B^{-1} expected from the average grain size (d) observed in the microscopy ("grey model" in Table 1) where significant bipolar contributions (κ_{bp}) were present at high temperatures. For BM and S-MS samples, the scattering terms $\tau_U^{-1} + \tau_{PD}^{-1} + \tau_B^{-1}$ were sufficient to explain the κ_l. However, the Te-MS required the introduction of dislocation scatterings τ_{DC}^{-1} and τ_{DS}^{-1} using values of the observed N_D and the fitted $B_{D,eff}$ as listed in Table 1, "grey + dislocation". The fitted $B_{D,eff}$ was within reasonable expectation,[33] especially considering the compounding effect leading to reinforcement of grain boundary dislocation scattering expected by Klemens.[16]

Now that we have concluded that τ_{DC}^{-1} and τ_{DS}^{-1} are required to model some of the grain boundary scattering in some samples, we can explore the possibility of this mechanism replacing the τ_B^{-1} term entirely to model all of the boundary scattering in all the samples studied.

Indeed, an equally satisfactory model exists by entirely replacing the τ_B^{-1} term in τ_{total}^{-1} of BM, S-MS, and Te-MS with τ_{DC}^{-1} and τ_{DS}^{-1} by using reasonable values of $B_{D,eff}$ and N_D as shown in Table 1 ("GBDS model"). The scattering from strain fields induced by the dislocations is stronger than that from dislocation cores.[16] Therefore the scattering by grain boundary dislocations (from both strain field and cores) is termed as grain boundary dislocation strain (GBDS) scattering for simplicity. The $B_{D,eff}$ and γ_1 values were kept unchanged from those acquired for Te-MS in the "grey + dislocation".

There are different kinds of grain boundaries, consisting of different kinds of defects, that produce the strain that scatters phonons. Nevertheless, it has been suggested that most if not all defects at grain boundaries can be described as some combination of dislocations.[16,34–39] Even if all types of grain boundaries cannot be entirely defined by dislocations, the usefulness of GBDS model requires only that dislocation strain is a dominant mechanism for boundary scattering.

Smaller grain size, d, which leads to increased scattering in τ_B^{-1} ("grey model") translates into a larger dislocation density (N_D) in "GBDS model" (Table 1). Besides, the stronger GBDS (given the same d) which could not be described in terms of phenomenological τ_B^{-1} was taken into account in a smaller s (greater N_D). Therefore, s for different samples were fit to the experimental κ_l (κ_{bp} is the same for both models) whose numbers are given in Table 1 ("GBDS model").

Previously, the N_D estimated from experimentally determined dislocation spacing in Te-MS and used in "grey + dislocation" was 2.0×10^{11} (cm^{-2}) (ref. 17), but with only a 10% increase in N_D, 2.2×10^{11} (cm^{-2}) (which is still physically reasonable),

Table 1 Theoretical total relaxation rate (τ_{total}^{-1}) considered for grey model and GBDS model

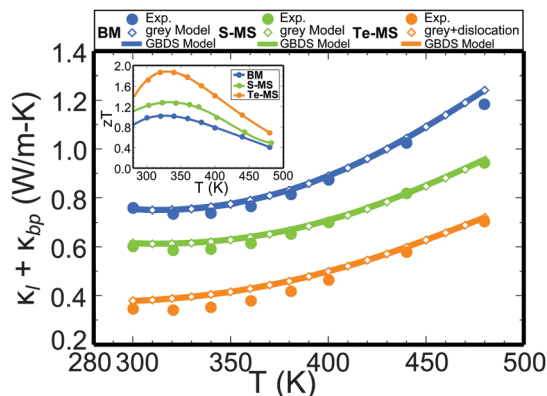| | $\tau_{total}(z)^{-1} = \tau_U^{-1} + \tau_{PD}^{-1} + \tau_i^{-1}$ | | | | | | | | | |
| | Grey model ("grey + dislocation" for Te-MS) | | | | | GBDS model | | | | |
Sample	τ_i^{-1}	$B_{D,eff}$ (Å)	d (μm)	s (nm)	N_D (cm^{-2})	τ_i^{-1}	$B_{D,eff}$ (Å)	d (μm)	s (nm)	N_D (cm^{-2})
BM	τ_B^{-1}	—	20	—	—	$\tau_{DC}^{-1} + \tau_{DS}^{-1}$	12.7	20	9.1	1.1×10^9
S-MS	τ_B^{-1}	—	0.3	—	—	$\tau_{DC}^{-1} + \tau_{DS}^{-1}$	12.7	0.3	21.5	3.1×10^{10}
Te-MS	$\tau_B^{-1} + \tau_{DC}^{-1} + \tau_{DS}^{-1}$	12.7	0.3	3.3	2.0×10^{11}	$\tau_{DC}^{-1} + \tau_{DS}^{-1}$	12.7	0.3	3.0	2.2×10^{11}

Fig. 1 Lattice and bipolar contribution to thermal conductivity of BM, S-MS, and Te-MS samples. Filled circle – experimental data, empty diamond – frequency-independent boundary scattering model (grey model), and solid line – grain boundary dislocation strain scattering model (GBDS model). Corresponding zT plot is given in the inset.

we can equally adequately describe the exceptionally low κ_l of Te-MS using "GBDS model" (orange solid line in Fig. 1). As anticipated, much weaker scatterings from GBDS in BM and S-MS are manifested in their calculated N_D (from fitted s), which are one or two orders magnitude smaller than that of Te-MS (Table 1) while in the range expected for polycrystalline materials.[40] Similar results can be applied to PbTe given removing boundary scattering by GBDS scattering can sufficiently explain the data like we show in Bi–Sb–Te.

Effect of scatterings from dislocation cores and strain field can be best understood when the spectral thermal conductivity (κ_s) is plotted.

$$\kappa_s = \frac{3k_B\omega^2}{2\pi^2 v}\tau(\omega) \qquad (10)$$

As described in the κ_s for S-MS (Fig. 2), while Umklapp scattering is effective at all frequencies, point defect scattering and boundary scattering (frequency-independent) only scatter high
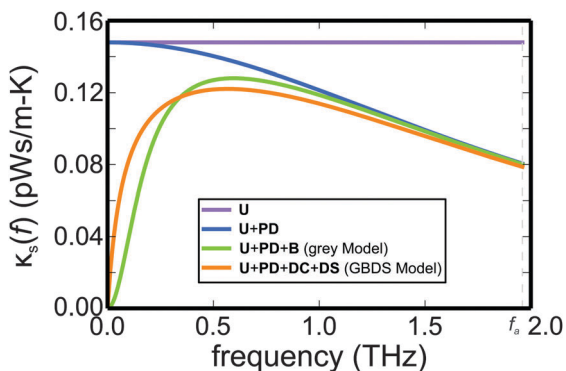
and low frequency phonons, respectively. Similar to the boundary scattering (green line – grey model), dislocation core and strain field scattering reduce thermal conductivity at low frequencies (orange line – GBDS model). Although the κ_s curves for the grey model (green line in Fig. 2) and the GBDS model (orange line in Fig. 2) do not coincide exactly in Fig. 2, their κ_l agree well (green diamond and green line in Fig. 1) with each other because the κ_l is the area under the κ_s curve.

Dislocation scattering model superior to boundary scattering model at low temperatures

In a recent study by Wang *et al.* on nanocrystalline Si,[7] it was shown that the traditional frequency-independent boundary scatterings fails to correctly predict the observed κ_l, even qualitatively. The grey model predicts a T^3 temperature dependence (green dotted line in Fig. 3) while the experimental measurements show a temperature dependence closer to T^2 at low temperatures.

Wang *et al.* were able to predict a T^2 temperature dependence using Born von Karman (BvK) model (group velocity is not constant), along with frequency-dependent boundary scattering relaxation rate ($\tau_{B,\omega}^{-1}$) approximated as

$$\tau_{B,\omega}^{-1} = c\frac{v\omega}{d}, \qquad (11)$$

where c is the dispersion relation dependent constant. The model in ref. 7, however, is phenomenological in that no mechanism was given for the frequency dependence.

Here we propose that GBDS may be the mechanism that leads to the frequency dependence. Because the GBDS model includes
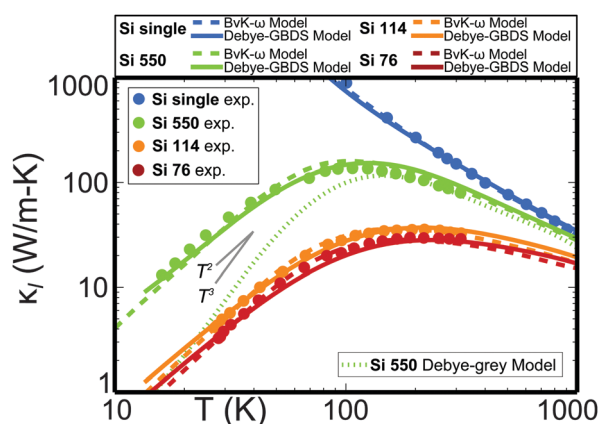

Fig. 2 Spectral thermal conductivity of S-MS. U (Umklapp), PD (Point-Defect), and B (frequency-independent Boundary scattering) are accounted for the calculation. For grey model, U, PD, and B are considered as relevant scattering mechanisms (green solid line). Meanwhile, in GBDS model B has entirely been replaced by scattering from dislocation cores (DC) and strain field (DS) (orange solid line).

Fig. 3 Lattice contribution to thermal conductivity of various Si samples. Si single (Si single crystal), Si 550 (nanocrystalline Si with 550 nm average grain size), Si 114 (nanocrystalline Si with 114 nm average grain size), and Si 76 samples (nanocrystalline Si with 76 nm average grain size) are plotted. Filled circle – experimental data, dashed line – Wang *et al.*'s Born von Karman model using frequency-dependent boundary scattering model ("BvK-ω model"), and solid line – Wang *et al.*'s Debye model using our GBDS scattering model in lieu of Wang *et al.*'s frequency-dependent boundary scattering model ("Debye-GBDS model"). For comparison, Wang *et al.*'s Debye model using frequency-independent boundary scattering ("Debye-grey model") for Si 550 is plotted in green dotted line.

both a dislocation strain field term with ω dependence and a dislocation core term with ω^3 dependence (for scattering relaxation rates) it cannot exactly reproduce the model in ref. 7, instead we show the GBDS model gives a satisfactory fit (Fig. 3). All the parameters and constants from Debye model in ref. 7 were re-utilized except for the boundary scattering, which was replaced by τ_{DC}^{-1} and τ_{DS}^{-1}. The γ_1 for Si was taken to be zero as Si is not an alloy, and for simplicity, lattice constant of Si (5.4 Å) was substituted for $B_{D,eff}$. Similar to the $(Bi_{0.25}Sb_{0.75})_2Te_3$ case, the dislocation spacing (s) was adjusted to match the experimental results. The fitted s (0.76–0.94 nm) for nanocrystalline Si was still above the minimum theoretical dislocation spacing (lattice constant $\sim$ 0.5 nm). The fit is nearly as good as the frequency-dependent BvK model in ref. 7 suggesting dislocation scattering may be the underlying mechanism in κ_l reduction due to grain boundary scattering.

Alloys

Experimental κ_l data of Si–Ge alloys by Savvides and Goldsmid[18,19] were also examined to show that the GBDS model can replace the grey model completely, which also revealed a new strategy for further suppressing κ_l. This mechanism utilizes the change in Grüneisen parameter that accompanies the compositional changes around dislocations in alloys.

The change in Grüneisen parameter (γ_1) of τ_{DS}^{-1} can strengthen or weaken the scattering due to GBDS depending on mass and volume mismatch between constituents of the alloy. The γ_1 can be estimated as[47]

$$\gamma_1 = \frac{V c_0 K}{k_B T_a}\left(\gamma \alpha^2 - \alpha\beta\right),\qquad(12)$$

with α and β being

$$\alpha = \frac{(V'-V)}{V},\quad \beta = \frac{1}{2}\frac{(M-M')}{M},\qquad(13)$$

where V', V, M', M, K, c_0, and T_a are the atomic volume of impurity, that of host, average atomic mass of impurity, that of host, bulk modulus of host, concentration of impurity in the alloy and the sample annealing temperature, respectively. For Te-MS, which is a $(Bi_{0.25}Sb_{0.75})_2Te_3$ alloy, the theoretical γ_1 is positive reinforcing the GBDS scattering.[17]

Savvides and Goldsmid[18,19] compared the relative change in κ_l from nanostructuring for different Si–Ge alloy compositions. In particular, they plotted the κ_l ratio of polycrystalline Si–Ge with different grain sizes (containing boundaries and point defects, $\kappa_{PD,B}$) relative to that of single crystal alloy (containing only point defects, κ_{PD}). Simply comparing two 30% alloys (Fig. 4) cannot provide any information on relative strength of the boundary scatterings in the alloys since the Fig. 4 plots the ratio of $\kappa_{PD,B}$ and κ_{PD}. In fact, according to Savvides and Goldsmid's calculated $\kappa_{PD,B}/\kappa_{PD}$ using the grey model (dashed lines in Fig. 4), less intense point-defect scattering in $Si_{0.7}Ge_{0.3}$ was held responsible for the lower $\kappa_{PD,B}/\kappa_{PD}$ of $Si_{0.7}Ge_{0.3}$.

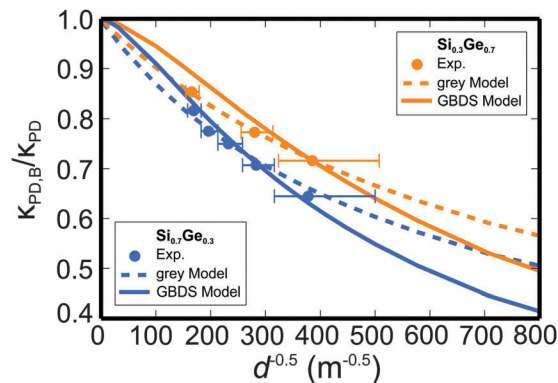Replacing the τ_B^{-1} in the Savvides and Goldsmid' model with the GBDS model, a reasonable fit to the experimental data

Fig. 4 Ratio of thermal conductivities whose departure from unity measures the boundary scattering effect. The ratio between $\kappa_{PD,B}$ (κ_l where point-defect and boundary scatterings are present) and κ_{PD} (κ_l where only point-defect scattering is present) for different grain sizes (d) is shown at 300 K. Plots in orange are for $Si_{0.3}Ge_{0.7}$ alloy and blue for $Si_{0.7}Ge_{0.3}$ alloy. Filled circle – experimental data, dashed line – Savvides and Goldsmid' model using the grey model, and solid line – Savvides and Goldsmid' model using our GBDS scattering model in lieu of the grey model (GBDS model).

was achieved (solid lines in Fig. 4) considering the uncertainty involved in determining the size of the grains (represented with error bars in Fig. 4).

For $Si_{0.7}Ge_{0.3}$ and $Si_{0.3}Ge_{0.7}$, $s = B_{D,eff} = 7$ Å (in eqn (8) and (9)) was adopted to produce the solid lines in Fig. 4. Even if the effective Burgers vector is larger than that normally expected for Si and Ge (5.4 Å and 5.5 Å, respectively), given the uncertainty of the models, we can still deduce that the GBDS model can provide an alternative to the Casimir model for boundary scattering.

If GBDS is indeed the correct mechanism for boundary scattering, the Klemens theory implies that the scattering due to impurity modulation around grain boundary dislocation strain field in Si–Ge alloys plays a vital role in further reducing the κ_l. The change in Grüneisen parameter (γ_1 in eqn (12)) of the Si–Ge alloys increase the overall Grüneisen parameter ($\gamma + \gamma_1$) in eqn (12) by 3.4 times for $Si_{0.7}Ge_{0.3}$ and about 2.1 times for $Si_{0.3}Ge_{0.7}$ reinforcing GBDS scattering accordingly. Now that the increased GBDS scattering becomes the dominant scattering mechanism, the discrepancy in $\kappa_{PD,B}/\kappa_{PD}$ for the two 30% alloys can be explained with the degree of impurity modulation (γ_1). The theoretical γ_1 for various thermoelectric materials are listed in Table 2.

Table 2 Theoretical change in Grüneisen parameter (γ_1) for thermoelectric materials

Material	α	β	γ	K (GPa)	T_a (K)	γ_1	$(\gamma + \gamma_1)/\gamma$
$(Bi_{0.25}Sb_{0.75})_2Te_3$	0.09[a]	−0.18	2.3[b]	45[d]	753[c]	1.1	1.49
$PbTe_{0.75}Se_{0.25}$	−0.15[a]	0.07	1.45[a]	39[d]	700[e]	1.4	1.99
$Pb_{0.97}Mg_{0.03}Te$	−0.02[a]	0.27	1.45[a]	39[d]	700[e]	0.03	1.02
$Si_{0.7}Ge_{0.3}$	0.13[f]	−0.79	0.56[a]	98[d]	1200[g]	1.3	3.32
$Si_{0.3}Ge_{0.7}$	−0.12[f]	0.31	0.76[a]	75[d]	1200[g]	0.8	2.07
$Mg_2Si_{0.7}Sn_{0.3}$	0.19[a]	−0.09	1.32[a]	49[d]	1000[h]	1.6	2.20

Taken from: [a] ref. 22. [b] Ref. 41. [c] Ref. 17. [d] Ref. 42. [e] Ref. 43. [f] Ref. 44. [g] Ref. 45. [h] Ref. 46.

Conclusions

In summary, straightforwardly applicable frequency-dependent phonon scattering due to dislocation strain in grain boundaries (GBDS model) can replace the most commonly used frequency-independent boundary scattering (grey model) to accurately predict the κ_l. Although the grey model is in wide use, it has been difficult to align with observed phenomena. The theoretical κ_l of Bi–Sb–Te, Si, and Si–Ge previously modelled with grey model were recalculated using GBDS model with equally satisfactory results. At low temperatures, boundary scattering is better described with scattering due to GBDS. We revisited Wang et al.'s thermal conductivity calculation (Debye model) using frequency-independent boundary scattering ($\sim T^3$) which deviated from experimental thermal conductivity ($\sim T^2$) at low temperatures. Accuracy of the Debye model is much improved when frequency-independent boundary scattering is changed to GBDS scattering. It is concluded that the scattering from GBDS is the more likely mechanism for the grain boundary scattering than the grey model derived for boundary scattering at the sample boundaries. Strengthening of the GBDS scattering via impurity modulation around dislocations in alloys opens possibilities for grain boundary engineering as a means toward more efficient thermoelectric materials.

Acknowledgements

Notes and references

1 G. J. Snyder and E. S. Toberer, *Nat. Mater.*, 2008, **7**, 105–114.
2 K. Biswas, J. He, I. D. Blum, C.-I. Wu, T. P. Hogan, D. N. Seidman, V. P. Dravid and M. G. Kanatzidis, *Nature*, 2012, **489**, 414–418.
3 W. J. de Haas and T. Biermasz, *Physica*, 1938, **5**, 619–624.
4 H. B. G. Casimir, *Physica*, 1938, **5**, 495–500.
5 R. Berman, *Thermal conduction in solids*, Clarendon Press, 1976.
6 R. Berman, *Proc. Phys. Soc., London, Sect. A*, 1952, **65**, 1029.
7 Z. Wang, J. E. Alaniz, W. Jang, J. E. Garay and C. Dames, *Nano Lett.*, 2011, **11**, 2206–2213.
8 J. M. Ziman, *Electrons and Phonons: The Theory of Transport Phenomena in Solids*, OUP, Oxford, 1960.
9 C. Hua and A. J. Minnich, *Semicond. Sci. Technol.*, 2014, **29**, 124004.
10 P. K. Schelling, S. R. Phillpot and P. Keblinski, *J. Appl. Phys.*, 2004, **95**, 6082–6091.
11 D. G. Cahill, P. V. Braun, G. Chen, D. R. Clarke, S. Fan, K. E. Goodson, P. Keblinski, W. P. King, G. D. Mahan, A. Majumdar, H. J. Maris, S. R. Phillpot, E. Pop and L. Shi, *Appl. Phys. Rev.*, 2014, **1**, 011305.
12 D. A. Young and H. J. Maris, *Phys. Rev. B: Condens. Matter Mater. Phys.*, 1989, **40**, 3685–3693.
13 K. Fuchs, *Math. Proc. Cambridge Philos. Soc.*, 1938, **34**, 100–108.
14 E. H. Sondheimer, *Adv. Phys.*, 2001, **50**, 499–537.
15 G. Chen, *J. Heat Transfer*, 1997, **119**, 220–229.
16 P. G. Klemens, in *Solid State Physics – Advances in Research and Applications*, ed. F. Seitz and D. Turnbull, Academic Press Inc., New York, 1958, pp. 1–98.
17 S. I. Kim, K. H. Lee, H. A. Mun, H. S. Kim, S. W. Hwang, J. W. Roh, D. J. Yang, W. H. Shin, X. S. Li, Y. H. Lee, G. J. Snyder and S. W. Kim, *Science*, 2015, **348**, 109–114.
18 N. Savvides and H. J. Goldsmid, *J. Phys. C: Solid State Phys.*, 1980, **13**, 4657.
19 N. Savvides and H. J. Goldsmid, *J. Phys. C: Solid State Phys.*, 1980, **13**, 4671.
20 P. G. Klemens, *J. Appl. Phys.*, 1968, **39**, 5304–5305.
21 J. Callaway, *Phys. Rev.*, 1959, **113**, 1046–1051.
22 E. S. Toberer, A. Zevalkink and G. J. Snyder, *J. Mater. Chem.*, 2011, **21**, 15843–15852.
23 E. F. Steigmeier and B. Abeles, *Phys. Rev.*, 1964, **136**, A1149–A1155.
24 B. Abeles, *Phys. Rev.*, 1963, **131**, 1906–1911.
25 H. Wang, A. D. LaLonde, Y. Pei and G. J. Snyder, *Adv. Funct. Mater.*, 2013, **23**, 1586–1596.
26 P. G. Klemens, in *Thermal Conductivity*, ed. R. P. Tye, Academic Press, London, 1969, pp. 1–68.
27 W. R. G. Kemp, P. G. Klemens, A. K. Sreedhar and G. K. White, *Proc. R. Soc. London, Ser. A*, 1956, **233**, 480–493.
28 J. N. Lomer and H. M. Rosenberg, *Philos. Mag.*, 1959, **4**, 467–483.
29 J. Zou, D. Kotchetkov, A. A. Balandin, D. I. Florescu and F. H. Pollak, *J. Appl. Phys.*, 2002, **92**, 2534–2539.
30 J. He, S. N. Girard, M. G. Kanatzidis and V. P. Dravid, *Adv. Funct. Mater.*, 2010, **20**, 764–772.
31 P. G. Klemens, *Proc. Phys. Soc., London, Sect. A*, 1955, **68**, 1113.
32 M. Stordeur and H. Sobotta, *The Proceedings of the First European Conference on Thermoelectrics*, Pereqrinus Ltd., London, 1988.
33 D. L. Medlin, K. J. Erickson, S. J. Limmer, W. G. Yelton and M. P. Siegal, *J. Mater. Sci.*, 2014, **49**, 3970–3979.
34 J. M. Burgers, *Proc. Phys. Soc.*, 1940, **52**, 23.
35 W. L. Bragg, *Proc. Phys. Soc.*, 1940, **52**, 54.
36 W. T. Read and W. Shockley, *Phys. Rev.*, 1950, **78**, 275–289.
37 R. Schindler, J. E. Clemans and R. W. Balluffi, *Phys. Status Solidi A*, 1979, **56**, 749–761.
38 A. P. Sutton, R. W. Balluffi and V. Vitek, *Scr. Metall.*, 1981, **15**, 989–994.
39 T. Schober and R. W. Balluffi, *Philos. Mag.*, 1970, **21**, 109–123.

40 C.-S. Man, X. Gao, S. Godefroy and E. A. Kenik, *Int. J. Plast.*, 2010, **26**, 423–440.

41 X. Chen, H. D. Zhou, A. Kiswandhi, I. Miotkowski, Y. P. Chen, P. A. Sharma, A. L. Lima Sharma, M. A. Hekmaty, D. Smirnov and Z. Jiang, *Appl. Phys. Lett.*, 2011, **99**, 261912.

42 O. Madelung, *Landbolt-Bornstein Numerical Data and Functional Relationships in Science and Technology*, Springer-Verlag, 1983.

43 Y. Pei, A. LaLonde, S. Iwanaga and G. J. Snyder, *Energy Environ. Sci.*, 2011, **4**, 2085–2089.

44 C. N. Singman, *J. Chem. Educ.*, 1984, **61**, 137.

45 D. M. Rowe, V. S. Shukla and N. Savvides, *Nature*, 1981, **290**, 765–766.

46 R. Schmidt, E. Case, J. Giles III, J. Ni and T. Hogan, *J. Electron. Mater.*, 2012, **41**, 1210–1216.

47 A. J. Friedman, *Phys. Rev. B*, 1973, **7**, 663.

This journal is © The Royal Society of Chemistry 2016